



Original article

Design and synthesis of a second series of triazole-based compounds as potent dual mPGES-1 and 5-lipoxygenase inhibitors

Maria Giovanna Chini^a, Rosa De Simone^a, Ines Bruno^{a,*}, Raffaele Riccio^a, Friederike Dehm^b, Christina Weinigel^c, Dagmar Barz^c, Oliver Werz^b, Giuseppe Bifulco^{a,**}

^a Department of Pharmaceutical and Biomedical Sciences, University of Salerno, Via Ponte Don Melillo, 84084 Fisciano (SA), Italy

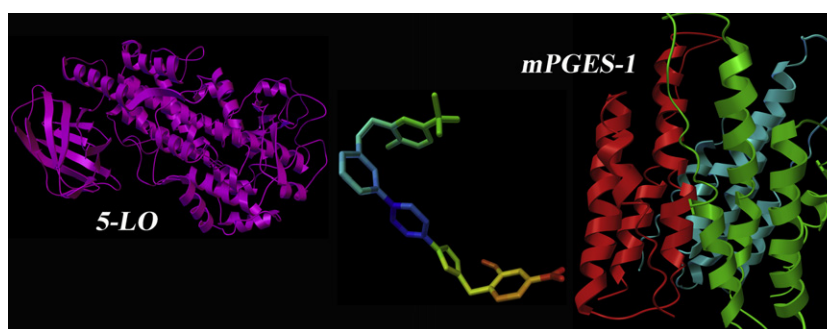
^b Pharmaceutical/Medicinal Chemistry, Institute of Pharmacy, Friedrich-Schiller-University, Philosophenweg 14, D-07743 Jena, Germany

^c Institute of Transfusion Medicine, University Hospital Jena, 07743 Jena, Germany

HIGHLIGHTS

- ▶ Design of 2nd series of new triazole-based compounds as mPGES-1 and 5-LO inhibitors.
- ▶ Synthesis of **2–16** performed by click chemistry and Suzuki cross-coupling reaction.
- ▶ Identification of **10, 11** and **14–15** as potent mPGES-1 inhibitors.
- ▶ **5, 10, 12** and **14–16** emerged as 5-LO inhibitors.

GRAPHICAL ABSTRACT



ARTICLE INFO

Article history:

Received 10 February 2012

Received in revised form

9 May 2012

Accepted 9 May 2012

Available online 18 May 2012

Keywords:

Triazole-based inhibitors

In silico screening

mPGES-1

5-Lipoxygenase

ABSTRACT

Microsomal prostaglandin E_2 synthase (mPGES)-1 and 5-lipoxygenase (5-LO) are pivotal enzymes in the biosynthesis of the pro-inflammatory PGE_2 and leukotrienes, respectively. The design and synthesis of a second series of mPGES-1 inhibitors based on a triazole scaffold are described. Our studies allowed us to draw a tentative SAR profile and to optimize this series with the identification of compounds **10, 11** and **14–15** which displayed potent mPGES-1 inhibition in a cell-free assay. In addition, compounds **5, 10, 12** and **14–16** also blocked 5-LO activity in cell-free and cell-based test systems, emerging as very promising candidates for the development of safer and more effective anti-inflammatory drugs.

© 2012 Elsevier Masson SAS. All rights reserved.

1. Introduction

For many years, the main strategy adopted to manage inflammatory disorders consisted in the inhibition of the key enzymes of

the prostaglandin (PG) biosynthetic pathway such as PLA_2 , COX-1 and COX-2; the latter was initially supposed to be a promising target for the development of therapeutic interventions owing to its inducible nature. Unfortunately, the long-term intake of COX-2 inhibitors (coxibs) is associated with severe cardiovascular toxicity and, thus coxibs are controversially discussed as therapeutics [1,2,3]. Lately, mPGES-1 enzyme, which catalyzes the last step of PGE_2 synthesis, has emerged as a valid alternative strategy in the struggle against inflammation [4]. In the last years, a plethora

* Corresponding author. Tel.: +39 089 969743; fax: +39 089 969602.

** Corresponding author. Tel.: +39 089 969741; fax: +39 089 969602.

E-mail addresses: brunoin@unisa.it (I. Bruno), bifulco@unisa.it (G. Bifulco).

of data have been gathered highlighting the key role played by this enzyme in inflammation-related disorders and its ability to affect PGE₂ synthesis only under inflammatory conditions, without suppressing the constitutive prostanoids involved in gastro-protection and in other crucial physiological functions [5,6,7]. Continuing our studies on small molecules able to block mPGES-1 activity, we recently reported the design and synthesis of a small collection of differently decorated disubstituted triazole derivatives able to interact with this target at micromolar concentrations. In the course of our investigations, we identified some interesting molecules able to inhibit mPGES-1 as well as other key enzymes within the arachidonic acid cascade such as 5-lipoxygenase (5-LO) and 5-LO-activating protein (FLAP) that are required for leukotrienes (LTs) formation [8]. The good qualitative coherence found in our previous work [8] between the biological results and the predictions of molecular docking calculations provided a satisfactory binding mode model of these triazoles with their respective biological targets (i.e., mPGES-1, 5-LO, and FLAP), gaining more information to envisage further structural optimizations of the basic template in accordance with the catalytic pocket requirements of the enzyme. In more detail, the previous investigations have disclosed the basic structure **1** [8] (Scheme 1), able to efficiently interact with key residues in the catalytic site, which needed to be further optimized for what concerns the substitution pattern on the biphenyl moiety and in order to provide a better binding affinity with the target enzyme. In line with these considerations, we have decided to leave the 2-nitro-4-carboxybenzyl moiety unchanged

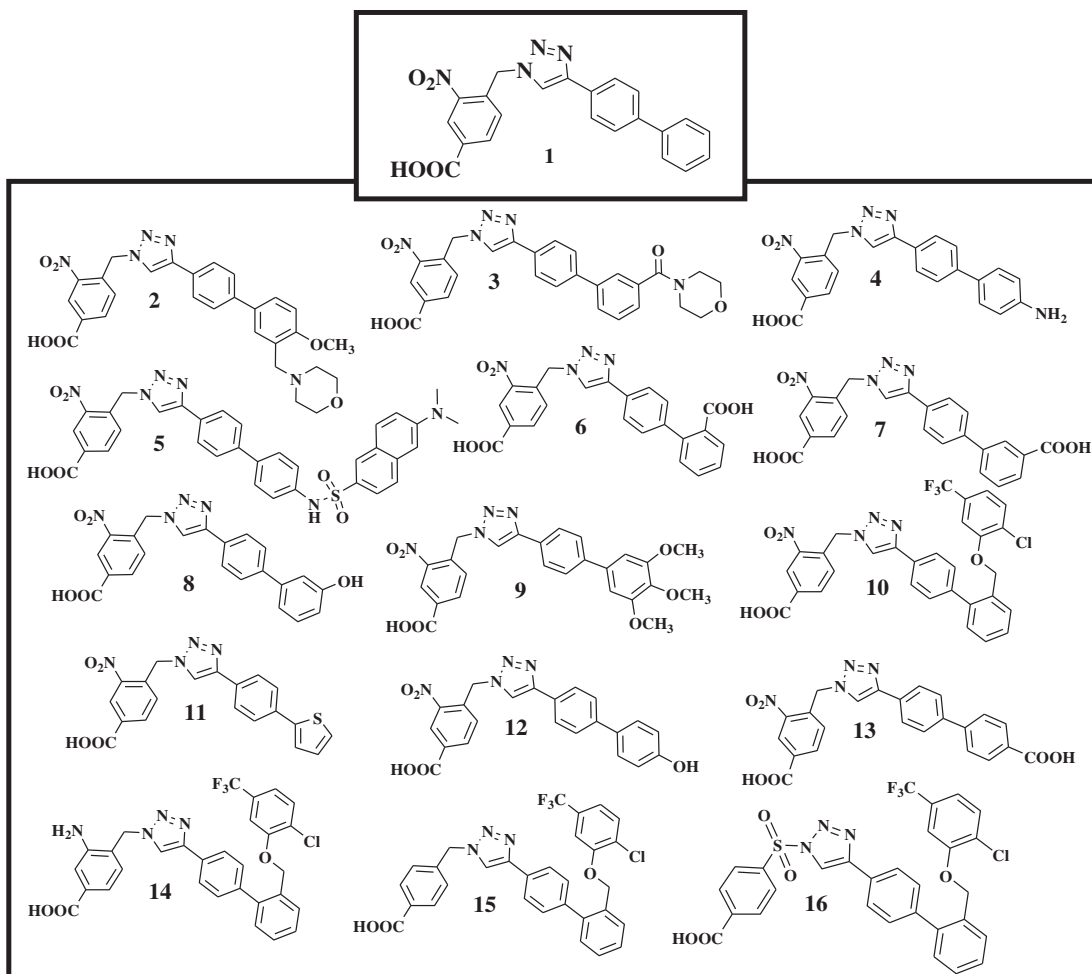
(Scheme 1) and to variously decorate the right hand portion of the molecule, coming to the identification of compound **11**, which retained mPGES-1 inhibition ability, and compound **10**, emerging as potent dual inhibitor of mPGES-1 and 5-LO enzymes. Building on these results, we have further refined the structure of compound **10**, leaving unmodified the right hand portion of the molecule and introducing some minor modifications on the left hand moiety, such as the reduction of the nitro group (compound **14**), the elimination of the ortho-substituent on the phenyl ring (compound **15**) and the insertion of a sulfonamide function between the phenyl and the triazole ring (compound **16**), reminiscent of the structural backbone showed by a triazole-based compound previously identified by us as potent dual inhibitor of mPGES-1 and 5-LO enzymes [8].

Here we report the computer-aided design, the synthesis and, the pharmacological profile of this second generation of triazoles derivatives; our findings provided new interesting hits shedding further light on the structural requirements needed for an optimal ligand–enzyme interaction.

2. Results and discussions

2.1. Docking studies

On the basis of the encouraging results regarding the rationalization of the inflammation processes related to natural products [9–13] and the design of new synthetic molecules [8,14,15], here we



Scheme 1. Structures of lead compound **1** and its derivatives.

report the design and the theoretical evaluation of a new significant set of molecules obtained by revisiting the lead compound **1** (See Scheme 1) [8]. In particular, we have substituted the scaffold of **1** with various groups of different size and hydrophobicity with the aim to improve potency and to trace a tentative SAR profile of this kind of potential anti-inflammatory drugs. As suggested from our previous work [8], the 2-nitro-4-carboxybenzyl moiety remarkably influences the activity of the triazole molecules, so this moiety was not altered for the molecules **2–13** (Scheme 1) combining it with small hydrophilic groups (COOH, OH, NH₂) at different positions (**4, 6–8, 12–13**, Scheme 1), or with hydrophobic groups with increasing size (**2–3, 5, 9–11**, Scheme 1) to understand their potential influence on biological profiles. Even if Jegerschöld et al. [16] have recently elucidated the electron crystallographic structure of closed inactive conformation of mPGES-1, owing to the lack of the experimental structure of the mPGES-1 open active form, for our docking calculations by Autodock4.2 software [17] we used the microsomal glutathione transferase 1 (MGST-1) [18] as model receptor. MGST-1 shows 38% sequence identity with the human mPGES-1 [19] and was successfully used in our previous work [8] and as template for molecular modeling and dynamics simulation [20,21]. The sequence alignment of these two MAPEG (membrane-associated proteins in eicosanoid and glutathione metabolism) superfamily enzymes [8,20] was used for the in silico screening analysis. Our results point out two different docking poses for these triazole-based potential mPGES-1 inhibitors: (a) the first one includes molecules with ortho- and/or meta-substituted biphenyl groups (**3, 6–8, and 10**, Fig. 1A), or with a smaller aromatic ring (**11**) as arms at position 4; (b) the second family relates to compounds containing the biphenyl portion with at least one substituent in the para position (**2, 4–5, 9, 12–13**, Fig. 1B). However, all the designed molecules accommodate in the ligand pocket situated in the region at the interface of the two mPGES-1 subunits (Fig. 1) [22,23] interacting with the highly conserved Arg110_{mPGES-1} (Arg113_{MGST-1}) [16,24–27] the key catalytic residue Arg126_{mPGES-1} (Arg129_{MGST-1}) [16,22,23], and establishing further contacts with Arg38, Leu39, Val65, Arg70, Tyr130, Thr131, Ser127 [22] (Arg37, Leu38, Val68, Arg73, Phe133, Phe134 and Gly130 in MGST-1, respectively).

On this basis, the substitutions at ortho, meta and para of the biphenyl arm with small hydrophilic groups cause a different pattern of hydrogen bonds with MGST-1 among **4, 6–8, 12–13** (See Fig. 2A). In particular, even though **6** and **7** have similar docking poses and both molecules are able to establish a π -cation interaction with Arg129 (Arg126_{mPGES-1}), the ortho COOH of **6** forms a hydrogen bond with Arg129 (Arg126_{mPGES-1}) while the meta

COOH of **7** interacts with Arg37 (Arg38_{mPGES-1}) (Fig. 2A). On the other hand, the para carboxybiphenyl arm of **13** interacts with aminoacids located at the bottom part of the ligand binding pocket establishing a π - π interaction with the Phe133 (Tyr130_{mPGES-1}), and moreover, its 2-nitro-4-carboxybenzyl moiety interacts with Asn81 and Lys25 (Fig. 2A). The same hydrogen bond pattern is also observed for the molecules **4, 8** and **12** (See Fig. 2B), where the OH (**12**) and/or NH₂ (**4**) group at para position of biphenyl arm do not allow the hydrogen bonds with Arg37 (Arg38_{mPGES-1}) and/or Arg129 (Arg126_{mPGES-1}), but allow the π - π interaction with Phe133 (Tyr130_{mPGES-1}) (See Fig. 2B); whereas for **8**, as like for **7**, the hydrogen bond with Arg37 and π -cation interactions with Lys67 and Arg129 are observed.

Regarding the molecules with bulky groups (**2–3, 5, 9, 10–11**, Scheme 1), depicted in Fig. 3, the different steric hindrance of the arms influences the positioning in the ligand binding site. In particular, the molecules with para (**5**) groups, or combined with meta (**2**) and/or ortho (**9**) substituents at biphenyl portion are in close contact with Gly130, Phe134 and establish π - π interactions with Phe133 (Tyr130_{mPGES-1}). On the other hand, even though **11** and compounds with bulkier arms (i.e. **3** and **10**) have similar docking poses, the thiophene ring of **11** allows peculiar van-der-Waals contacts with Ala32 and Val68, and a further π -cation interaction with Lys67; while **10** with respect to **3** establishes additional π -cation interactions with Arg129 (Arg126_{mPGES-1}) and Arg37 (Arg38_{mPGES-1}) and hydrophobic contact with Pro125.

From the above considerations, we have identified the differences between these two families of molecules where the substituents position on the arms influences the pattern of hydrophobic interactions and/or the hydrogen bonding. For these reasons, we decided to undertake the synthesis of the designed molecules (all within the lowest free energy of binding ($E_{\text{binding}} < -7$ kcal/mol) as the starting point for obtaining preliminary experimental results based on the evaluation of the bioactivity of this small set of compounds with the aim of a deeper understanding of the key features of new mPGES-1 triazole-based inhibitors. On the basis of the biological results, we have decided to further improve and refine the structure of the most active molecule **10** that was recognized as new lead compound (see Biological section) for the design of triazole-based mPGES-1 inhibitors. In particular, we have aimed to improve the biological activity of new lead compound **10**, modifying its 2-nitro-4-carboxybenzyl moiety (**14–16**) taking into account our previous considerations [8]. As shown in Fig. 4, the molecule **15** assumes the same docking pose with respect to **10**, where the elimination of the NO₂ group

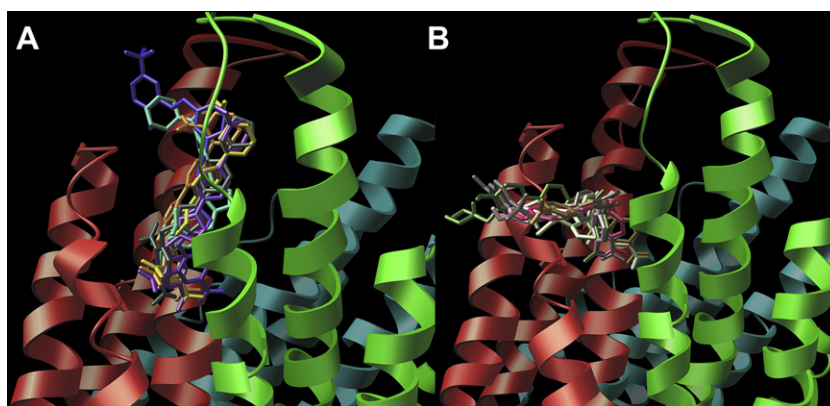


Fig. 1. Two different spatial arrangements of triazole-based compounds **1–13** in the binding site of MGST-1. (A) Superposition of compounds **3** (emerald), **6** (orange), **7** (yellow), **8** (purple), **10** (blue) and **11** (dark green). (B) Superposition of **2** (green), **4** (pink), **5** (gray), **9** (light green), **12** (light pink) and **13** (light brown). (For interpretation of the references to colour in this figure legend, the reader is referred to the web version of this article.)

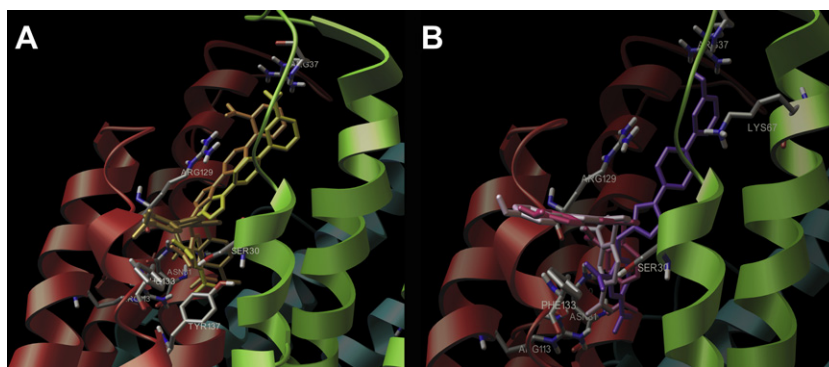


Fig. 2. (A) Three dimensional models of the different hydrogen bond patterns of **6** (orange), **7** (yellow), and **13** (light brown) with MGST-1 binding site. (B) Three dimensional models of the different hydrogen bond patterns of **8** (purple), **4** (pink) and **12** (light pink) with MGST-1 binding site. In both the figures the crucial aminoacids of MGST-1 receptor are depicted by stick and balls (by atom type: C, gray; O, red; N, dark blue; and S, yellow). (For interpretation of the references to colour in this figure legend, the reader is referred to the web version of this article.)

influence the strength of the H-bonding with the Arg113 (Arg110_{mPGES-1}), while the π -cation interactions with Arg129 (Arg126_{mPGES-1}) and Arg37 (Arg38_{mPGES-1}), and most of the hydrophobic interactions are maintained. On the other hand, the chemical reduction of the nitro group to NH₂ for **14**, and the insertion of a sulfonamide function between the phenyl and the triazole ring at **1** yielding **16** causes a different positioning of the compounds compared to **10**, and a shifting of the bulky arm at C-4 of the triazole ring in the MGST-1 ligand pocket. In particular, the NH₂ group of **14** establishes two additional hydrogen bonds acting as H-bond donor with the carbonyl oxygen of Gly223 and N ^{δ 1} of His75, making also possible the hydrogen bond between the triazole ring with the hydroxyl group of Thr33, and hydrophobic interactions of the halogenated benzene with Gly130, Pro127 and Gln126. On the other hand, the sulfonamide function of **16** only forms a hydrogen bond with the OH moiety of Thr33.

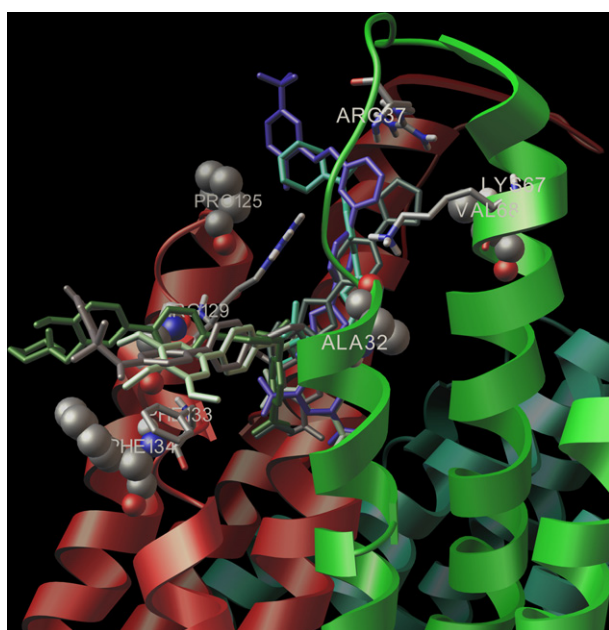


Fig. 3. Three dimensional models of the different hydrogen bond patterns and peculiar hydrophobic interactions of **2** (green), **3** (emerald), **5** (gray), **9** (light green), **10** (blue), and **11** (dark green) with the MGST-1 binding site. The crucial aminoacids of MGST-1 are depicted by stick and balls and CPK (by atom type: C, gray; O, red; N, dark blue; and S, yellow). (For interpretation of the references to colour in this figure legend, the reader is referred to the web version of this article.)

On this basis, we have synthesized these compounds and assessed the biological activity to prove our theoretical findings.

2.2. Chemistry

For the synthesis of analogs **2–16**, the retro-synthetic approach suggested us to obtain the triazole ring through the copper-catalyzed 3 + 2 Huisgen's cycloaddition between the appropriate terminal alkynes and azides [27], while to generate the differently decorated biphenyl systems we relied on the Suzuki cross-coupling reaction [28] that afforded the desired compounds (Scheme 2).

In more detail, the triazole rings were generated through the condensation between the appropriate terminal alkynes and the azides following two different synthetic procedures. Specifically, when we started from the commercially available azide **17**, containing a strong electron-withdrawing group such as the sulfonyl function that could drive the reaction toward undesired by-products formation, decreasing the yields of our expected cycloadduct [29], we carried out the reaction with 1-bromo-4-ethynylbenzene **18** in dry chloroform at 0 °C in presence of 2,6-lutidine as base (Scheme 3) [30]. On the contrary, when the

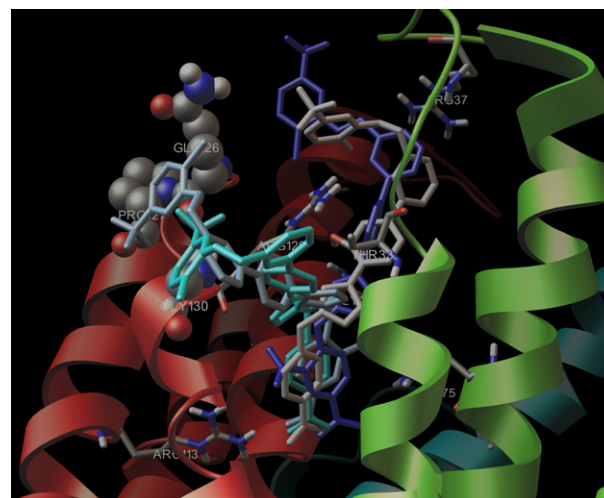
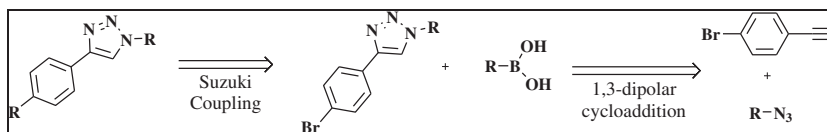


Fig. 4. Three dimensional models of the different hydrogen bond patterns and peculiar hydrophobic interactions of **10** (blue), **14** (light blue), **15** (white), and **16** (cyan) with MGST-1 binding site. The crucial aminoacids of MGST-1 receptor are depicted by stick and balls and CPK (colored by atom type: C, gray; O, red; N, dark blue; and S, yellow). (For interpretation of the references to colour in this figure legend, the reader is referred to the web version of this article.)

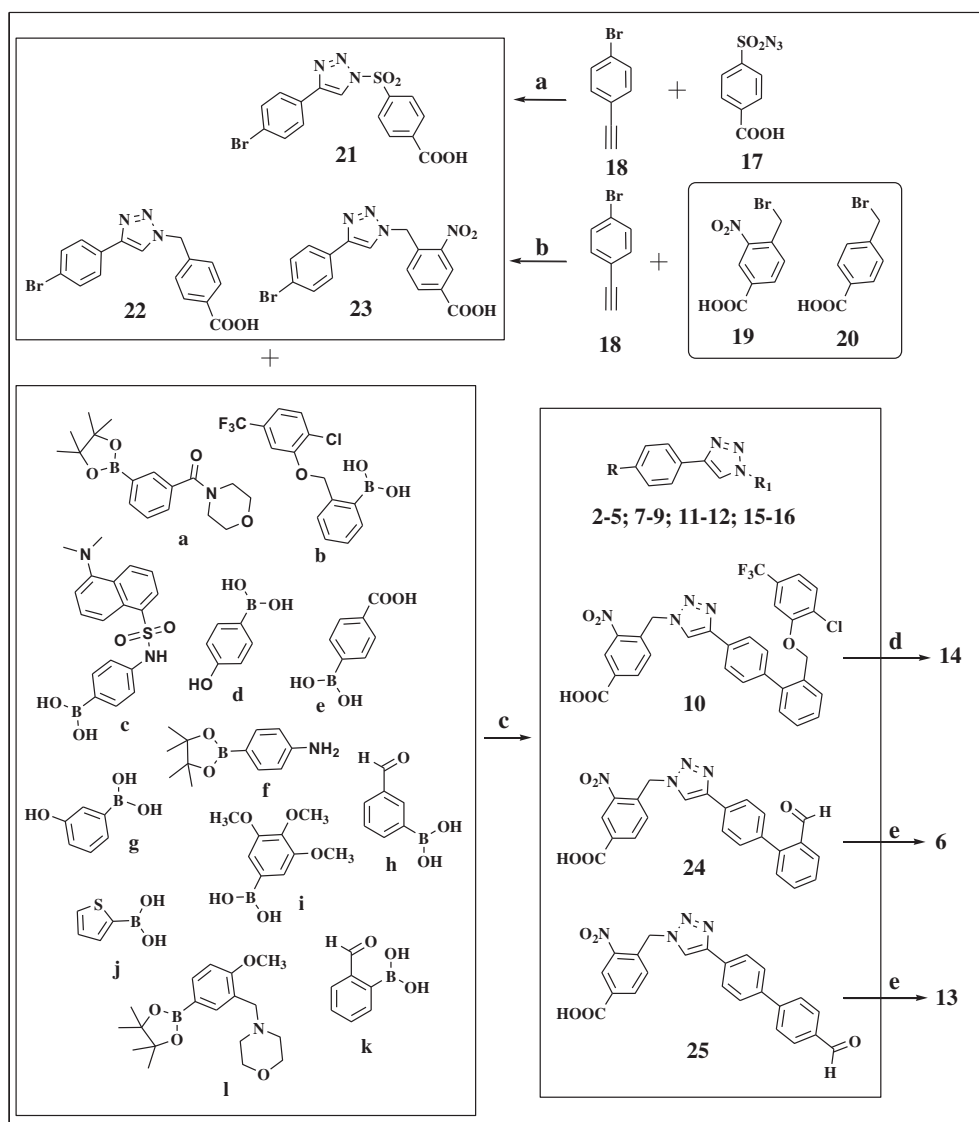


Scheme 2. Retro-synthetic approach for the synthesis of derivatives **2–16**.

azides were not available, the microwave irradiation technique provided a faster way to obtain the desired triazole intermediates **22–23** (Scheme 3) in a one-pot reaction implicating the *in situ* generation of azides starting from the corresponding halides **19–20** and sodium azide (Scheme 3) [31]. The 1,3-dipolar cycloaddition required the presence of Cu(I) as catalyst for directing the selective formation of 1,4-disubstituted triazoles [32]. The triazole intermediates **21–23**, obtained from the first step, were further subjected to the Suzuki cross-coupling reaction with the appropriate boronic acid **a–l** following the experimental conditions previously optimized by us [33], requiring the use of Pd(dppf)Cl₂ as catalyst and CsF as base in a mixture of tetrahydrofuran/water (THF/H₂O) 1:1, under microwaves irradiation; the desired final

compounds **2–5**, **7–12** and **15–16** and the advanced intermediates **24–25** (Scheme 3) were obtained in satisfactory yields.

The nucleophilic partners employed in the Suzuki coupling are all commercially available except for pinacol esters **a** and **l**. These last were obtained, as shown in Scheme 4, starting from the appropriate boronic acids **26** and **27** which were firstly protected as pinacol esters **28** and **29**, in order to facilitate the purification step on silica column, and finally were converted in the boronate **l** through a reductive amination of **29** in presence of morpholine and in the amide **a** subjecting **28** to an amidation with morpholine using triethylamine (TEA) as base, N-hydroxybenzotriazole (HOBt) and N,N-dicyclohexylcarbodiimide (DIC) as carboxylate activators and N,N-dimethylformamide (DMF) as solvent.



Scheme 3. Synthetic protocol employed to generate derivatives **2–16**.^a Reagents and conditions: (a) CuI, 2,6-lutidine, CHCl₃ dry, 12 h, 0 °C. (b) CuSO₄, Cu(0), NaN₃, t-BuOH/H₂O 1:1, microwaves, 25 min (c) CsF, Pd(dppf)Cl₂, H₂O/THF 1:1, microwaves, 25 min (d) SnCl₂, EtOH, 80 °C, 30 min (e) KMnO₄, Na₂HPO₄, CH₃OH, r.t., 1.5 h.

Finally, for the synthesis of compounds **6** and **13**, we experienced a low reactivity of 4- and 2-carboxy-boronic acids in the Suzuki coupling in the course of our trials, and thus we decided to subject the intermediates **24–25**, appropriately synthesized for the purpose, to oxidation with KMnO_4 and Na_2HPO_4 in CH_3OH as solvent for converting the aldehyde into the corresponding carboxylic acid group. On the other hand, to obtain compound **14** we reduced the nitro group of compound **10** to the corresponding amine employing SnCl_2 in ethanol (EtOH) as solvent (Scheme 3). Before submitting the synthesized compounds **2–16** to the biological assays, their purities (>95%) were verified by Agilent Technologies 1200 series high-performance liquid chromatography (HPLC) with ultraviolet (UV) detection at 280 nm (method: Jupiter C-18 column, 250 mm \times 4.60 mm, 5 μm , 300 \AA ; 1.0 mL/min flow rate; 5–100% in 30 min of 0.1% TFA/ CH_3CN -0.1% TFA/ H_2O).

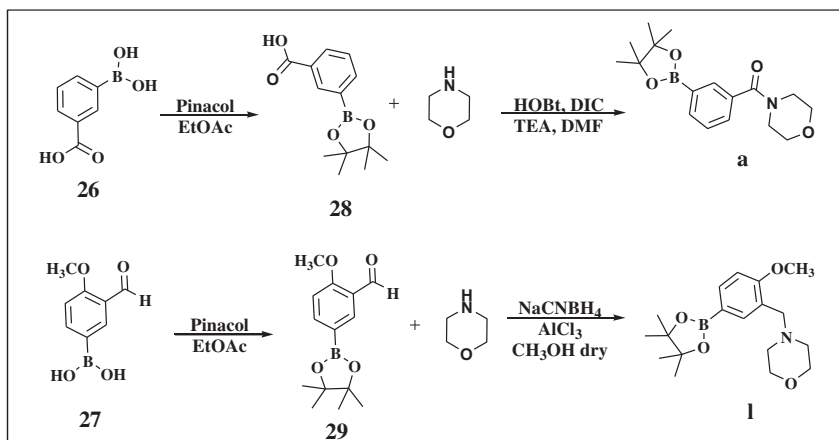
2.3. Biological activity

In order to assess the ability of the test compounds to interfere with mPGES-1 activity, a well-established cell-free assay [4,34] was applied, where microsomes of interleukin-1 β -stimulated A549 cells were used as source for human mPGES-1 enzyme and PGH_2 (20 μM) as substrate for mPGES-1. The mPGES-1 inhibitor MK-886 (IC_{50} = 2.4 μM) was used as a reference compound [35] that inhibited the enzymatic reaction by $82 \pm 6.4\%$ at a concentration of 10 μM (not shown). The results of the assessment of the mPGES-1-inhibitory activities and some SAR comments of compounds **1–16** are given in Table 1. For compound **1**, carrying a biphenyl, an IC_{50} value of 3.2 μM was obtained, which is in agreement with our previous finding [8]. Bioisosteric replacement of the 4-phenyl within the biphenyl of **1** by thiophene, yielding **11**, was essentially tolerated (IC_{50} = 5.5 μM). However, substitution of the 4-phenyl within the biphenyl by polar residues like 3'- or 4'-OH (compounds **8** and **12**, respectively), 4'- NH_2 - (compound **4**) or 2'-, 3'- or 4'-COOH groups (compounds **6**, **7** and **13**, respectively) was clearly detrimental with IC_{50} values > 10 μM . In fact, the carboxy-substituted analogs **6**, **7**, and **13** completely failed to significantly inhibit mPGES-1 up to 10 μM . Since we aimed to identify potent mPGES-1 inhibitors with improved efficiency versus the lead compound **1** (i.e., IC_{50} values < 3.2 μM), higher concentrations than 10 μM were not tested as they appeared not pharmacologically relevant and encouraging. Insertion of 3'-morpholino residues together with a methoxy moiety (compound **2**) or bridged via a keto group (compound **3**) also caused strong loss of potency. Substitution of the 4-phenyl moiety by three methoxy groups in 3'-, 4'-, and 5'-position in compound **9** retained some inhibitory

activity (45.7% inhibition at 10 μM) but still the IC_{50} was > 10 μM . Also the insertion of the bulky naphthyl sulfonamide in 4'-position, yielding compound **5**, did not improve the potency. In contrast, when the bulky, halogenated phenylether was inserted in 2'-position (compound **10**), a significant improvement in the potency was obtained, with an IC_{50} value = 1.2 μM . Next, the influence of the 2-nitro group within the 4-carboxybenzyl moiety on mPGES-1 inhibition was investigated. Omission of the 2-nitro moiety (resulting in compound **15**) slightly improved mPGES-1 inhibition (IC_{50} = 1.0 μM). Replacement of the 2-nitro function by an amino moiety further increased the efficiency and the respective compound **14** exhibited an IC_{50} value of 0.68 μM , representing the most potent mPGES-1 inhibitor within this study. Exchange of the methylene bridge next to the triazole of **15** by a sulfone moiety (compound **16**) again abolished the gain of potency.

It was shown in several studies that mPGES-1 inhibitors often also act on related enzymes within the arachidonic acid cascade such as COX or 5-LO enzymes, and it was proposed that dual inhibition of mPGES-1 and 5-LO might be beneficial for therapeutic use, in particular because of an expected lower risk of side effects [7,36]. Therefore, and based on the previous observation that compound **1** also efficiently inhibits 5-LO [8], we assessed the potential of the above-mentioned compounds for inhibition of human 5-LO in well-established cell-free and a cell-based models [8,34,37]. Interestingly, inhibition of 5-LO in both the cell-free and the cell-based test systems essentially correlated with the interference of the compounds with mPGES-1. Thus, compounds **2–9**, **12** and **13** that all failed or hardly inhibited mPGES-1 were also modest 5-LO inhibitors (IC_{50} > 10 μM), except the sulfonamide **5** and the 4'-OH biphenyl analog **12** of compound **1** that suppressed 5-LO in the cell-free (but not in the intact cell) assay with IC_{50} = 6.1 and 6.8 μM , respectively. On the other hand, the potent mPGES-1 inhibitors **10**, **14** and **15** efficiently inhibited 5-LO activity with IC_{50} values in the range of 0.9–2 μM in the cell-free and 2.0–5.3 μM in the cell-based assay, respectively. One exception was the sulfone **16**, which was inactive for mPGES-1 but a potent 5-LO inhibitor with IC_{50} = 1.9 and 1.2 μM in cell-free and cell-based systems, respectively. Obviously, the sulfone or sulfonamide moieties (in compounds **16** and **5**, respectively) govern 5-LO inhibition but are detrimental for interference with mPGES-1. Taken together, compound **14** turned out to be the most potent dual mPGES-1/5-LO inhibitor out of these series with 4- and 7-fold lower IC_{50} values versus the parental lead compound **1**.

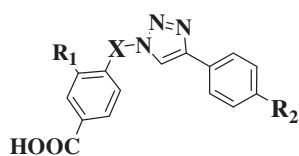
To rationalize the inhibitory activity of **5**, **10**, **12** and **14–16** on 5-LO by means of molecular docking, we used the crystal structure of stable 5-LO recently reported by Newcomer and co-workers [38]. We considered the molecules as possible nonredox-type 5-LO



Scheme 4. Synthetic protocol to generate pinacol esters **a** and **I**.

Table 1

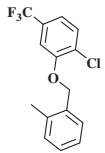
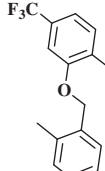
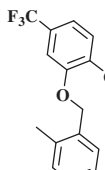
Inhibition of mPGES-1 and 5-LO, and SAR comments on mPGES-1 inhibitory activity of the tested compounds.



Comp.	R ₁	X	R ₂	mPGES-1 (IC ₅₀ [μM]; remaining activity at 10 μM)	SAR comments on the mPGES-1 inhibitory activity	5-LO (IC ₅₀ [μM]; remaining activity at 10 μM)	
						cell-free	cell-based
1	NO ₂	CH ₂		3.2	Lead compound	6.7	9.2
2	NO ₂	CH ₂		> 10 (87.4 ± 9.1%)	3'-morpholino residues together with a methoxy moiety; potency lost	> 10 (84.9 ± 11.1%)	> 10 (111.1 ± 8.4%)
3	NO ₂	CH ₂		> 10 (88.9 ± 4.2%)	3'-morpholino residues bridged via keto group; potency lost	> 10 (62.7 ± 12.2%)	> 10 (125.0 ± 12.0%)
4	NO ₂	CH ₂		> 10 (65.5 ± 5.1%)	polar residues; potency lost	> 10 (63.5 ± 11.3%)	> 10 (100.1 ± 5.3%)
5	NO ₂	CH ₂		> 10 (72.5 ± 4.3%)	bulky naphthyl sulfonamide in 4'-position did not improve the potency	6.1	> 10 (96.5 ± 7.3%)
6	NO ₂	CH ₂		> 10 (94.1 ± 8.5%)	polar residues; strong lost of potency	> 10 (75.3 ± 13.1%)	> 10 (65.9 ± 4.7%)
7	NO ₂	CH ₂		> 10 (82.1 ± 2.5%)	polar residues; strong lost of potency	> 10 (74.7 ± 9.6%)	> 10 (123.8 ± 5.5%)
8	NO ₂	CH ₂		> 10 (55.6 ± 0.8%)	polar residues, potency lost	> 10 (80.2 ± 2.7%)	> 10 (113.9 ± 10.1%)
9	NO ₂	CH ₂		> 10 (54.3 ± 1.5%)	methoxy groups in 3'-, 4'-, and 5' retained some inhibitory activity	> 10 (64.3 ± 11.8%)	> 10 (90.2 ± 9.3%)
10	NO ₂	CH ₂		1.2	bulky, halogenated phenylether is a preferred substituent; improvement of potency	2.0	5.3
11	NO ₂	CH ₂		5.5	thiophene ring; potency retained	> 10 (52.2 ± 9.6%)	> 10 (89.7 ± 2.8%)
12	NO ₂	CH ₂		> 10 (74.2 ± 1.8%)	polar residues; potency lost	6.8	> 10 (108.3 ± 1.1%)
13	NO ₂	CH ₂		> 10 (93.0 ± 21.2%)	polar residues; strong loss of potency	> 5 (62.7 ± 12.7%) [5 μM]	> 5 (90.9 ± 8.6%) [5 μM]

(continued on next page)

Table 1 (continued)

Comp.	R ₁	X	R ₂	mPGES-1 (IC ₅₀ [μM]; remaining activity at 10 μM)	SAR comments on the mPGES-1 inhibitory activity	5-LO (IC ₅₀ [μM]; remaining activity at 10 μM)	
						cell-free	cell-based
14	NH ₂	CH ₂		0.68	bulky, halogenated phenylether together with 2-amino group is very potent; highly active. New lead compound	0.9	2.1
15	H	CH ₂		1.0	bulky, halogenated phenylether with omission of the 2-nitro moiety; slightly less active as compared to 14	1.47	2.0
16	H	SO ₂		> 10 (78.6 ± 9.6%)	bulky, halogenated phenylether together with sulfone bridge; potency lost	1.96	1.2

inhibitors [39,40] since it does not show any features of a redox-active agent or properties of an iron-ligand. Because the 5-LO was crystallized without ligand [38], we referred to the model interactions described by Wouters et al. [41], which was already successfully used by us [8] and other research groups [42,43], and to the binding mode descriptions recently reported by Banoglu et al. [44] for nonredox-type 5-LO inhibitors. In our models, in fact, all the molecules interact with a binding site formed by Arg411, Ile406, Phe177, Lys409, Tyr181, Leu607, Leu414, Leu420, Trp599, Asn425, Gln363, Phe421, and Leu368 [41–44] however, the different size of the second arms influence their binding mode on the protein molecular surface. As depicted in Fig. 5, for all six potential inhibitors, the –COOH group and the triazole ring of 2-nitro-4-carboxybenzyl form a hydrogen bond with Arg596 and a π -cation interaction with Lys243, respectively. On the other hand, the –NH₂ group of 14 allows a further hydrogen bond with the carbonyl oxygen of Gly419 and the carboxylic group in the side chain of Asp422, while the oxygen of the halogenated arms of 10, 14–16 act as H-bond acceptors with the NH^{e22} of Gln413, and moreover, they are able to establish electrostatic interactions with Lys409 and Lys173 by the chlorine atom. Furthermore, even though 5 shows a different binding mode compared to the other compounds, it establishes hydrophobic contacts with Arg411, Asn148, Cys159, Glu417, Ile415, Lys158, and Trp147.

All these interactions provide complexes with an increased predicted stability that is fully compatible with the results of the experimental biological assays, giving a good rationalization of the 5-LO inhibitory activity of 5, 10, 12, 14–16.

2.4. SAR profile for the designed molecules 2–16 on the mPGES-1 inhibitory activity

Starting from the lead compound 1, the simple substitution of the phenyl group with the small aromatic ring as thiophene at R₂ (Scheme 5) yielding 11, positively influences the inhibitory activity on mPGES-1 (Table 1). On the other hand, the triazole compounds with a phenyl ring at R₂ substituted by small polar groups at ortho, meta and para positions (4, 6–8 and 12–13) show a decrease of

potency. In fact, in this small group of molecules, all the compounds presenting a COOH group (6, 7 and 13) completely failed the mPGES-1 inhibition. In contrast, compound 9, having a three methoxy phenyl ring at R₂ acts as a weak inhibitor. Furthermore, also the triazole-based compounds showing at R₂ a phenyl ring substituted with bulky groups at meta and/or para position as 2, 3 and 5 are significantly less potent with respect to the lead compound 1 underlining the negative effect of the steric hindrance in these positions on the biological activity (Table 1). On the contrary, when the phenyl ring at R₂ is substituted with the bulky halogenated phenylether (10), the activity increases with respect to the lead compound 1. Moreover, the presence of the NO₂ and/or NH₂ may modulate the activity, in fact both 14 and 15 are new potent mPGES-1 inhibitors; on the contrary compound 16, where the substitution of the methylene bridge with the SO₂ group causes a complete loss of potency, suggesting the critical role of the alkylic linker on the biological activity. In conclusion, in Scheme 5 a tentative SAR profile of these triazole-based compounds is reported.

3. Conclusions

We have designed, synthesized, and performed biological evaluation of a small set of potential anti-inflammatory triazole derivatives (2–16), obtained by modifying the scaffold of lead compound 1 previously reported by us. Our rational design had the aim to increase the interaction efficiency with the ligand binding site, and it was helpful for the comprehension of the key features of new mPGES-1 triazole-based compounds to direct the synthesis toward the most promising mPGES-1 inhibitors. In particular, the different substitutions on the arms at position 4 of the triazole ring caused a great disparity in activity among this class of compounds, where only 10, 11, 14 and 15 exhibit significant mPGES-1 inhibitory activity determining the critical features necessary for the optimal contact modes with MGST-1 binding pocket. By mean of molecular docking, in fact, a satisfactory explanation of the putative binding mode for these triazole-based mPGES-1 inhibitors was provided. In conclusion, we have proven the triazole ring with 2-nitro, and/or ammino-2, and/or carboxybenzyl moiety at position 1 combined with two aromatic

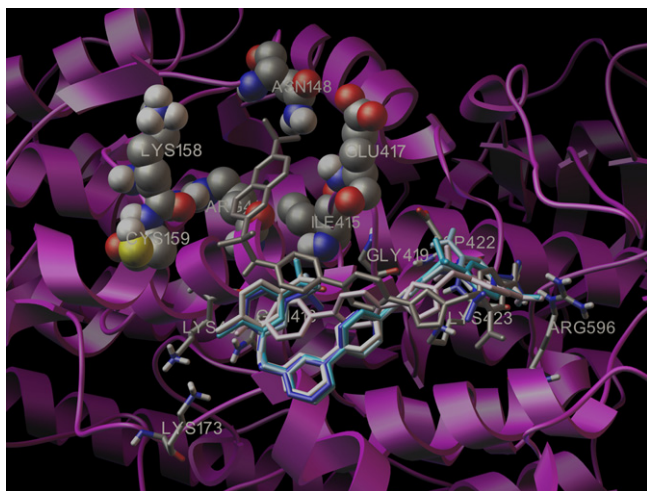


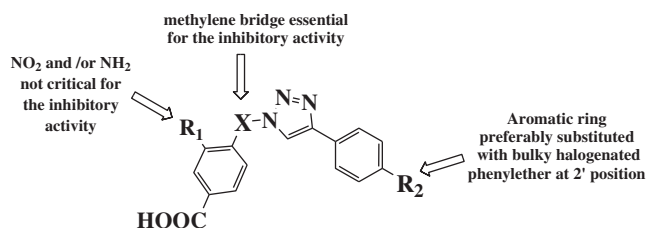
Fig. 5. Three dimensional models of the **5** (gray), **10** (blue), **12** (light pink), **14** (light blue), **15** (white), and **16** (cyan) with 5-LOX. The 5-LOX is represented by molecular surface (A) (colored by atom type: C, gray; O, red; N, dark blue; and S, yellow) and purple ribbon (B). The crucial aminoacids of 5-LOX are depicted by stick and balls and CPK (colored by atom type: C, gray; O, red; N, dark blue; and S, yellow). (For interpretation of the references to colour in this figure legend, the reader is referred to the web version of this article.)

rings at position 4, and/or with an ortho-substituted biphenyl with bulky, halogenated phenylether as new scaffold utilizable in the rational design of innovative mPGES-1 inhibitors. Moreover, the ability of the compounds to interfere with mPGES-1 significantly correlates with inhibition of 5-LO; in this regard we were able to rationalize the inhibitory activity of **5**, **10**, **12**, and **14–16** on 5-LO at the molecular level. As a major result, we present compound **14** as a novel potent dual mPGES-1/5-LO inhibitor with IC_{50} values in the sub-micromolar range. Whether or not these *in-vitro* properties of compound **14** translate into anti-inflammatory activity *in vivo* is a challenging question and currently under investigation along with detailed analysis of its molecular pharmacology.

4. Experimental section

4.1. Computational details

We performed molecular docking calculations by Autodock4.2 software [17] on 4x AMD Opteron SixCore at 2.4 GHz. For all the docking studies on MGS1 (pdb code: 2H8A) [18] a grid box size of $98 \times 98 \times 126$ with spacing of 0.375 \AA between the grid points, and centered at $-43.667 (x)$, $33.493 (y)$ and $2.656 (z)$ was used covering the active site of the target. For all the docked structures, all bonds were treated as active torsional bonds. To achieve a representative conformational space during the docking studies and for taking into account the variable number of active torsions, 10 calculations consisting of 256 runs were performed, obtaining 2560 structures for each ligand. The Lamarckian genetic algorithm (LGA) was employed for docking calculations, choosing an initial population of



Scheme 5. SAR summary profile for the designed compounds **2–16**.

600 randomly placed individuals. The maximum number of energy evaluations and of generations was set up to 5×10^6 and to 6×10^6 respectively. Results differing by less than 3.5 \AA in positional root-mean-square deviation (RMSD) were clustered together and represented by the result with the most favorable free energy of binding. On the other hand, for the rationalization of the binding mode of **5**, **10**, **12**, **14–16** with 5LO (pdb code: 3O8Y) [38] we used Autodock Vina software [45] choosing a grid box size of $30 \times 28 \times 28$, with spacing of 1.000 \AA between the grid points, and centered at $-11.146 (x)$, $66.57 (y)$ and $0.523 (z)$ covering the active site of the macromolecule. For the docking studies, we used an exhaustiveness of 8 with maximum energy difference of 3 kcal/mol between the best binding mode and the worst one displayed. Illustrations of the 3D models were generated using the Python software [46].

4.2. Synthesis of compounds **2–16**

4.2.1. Methods and materials

All water and air sensitive reactions were carried out under an inert atmosphere (N_2) in oven- or flame-dried glassware. CH_2Cl_2 , $CHCl_3$ and THF were distilled from CaH_2 immediately prior to use. Water was degassed under vacuum (10 mbar). All reagents were used from commercial sources (Sigma–Aldrich) without any further purification. Microwave reactions were performed on a CEM Discover® single mode platform using 10 mL pressurized vials.

Reactions were monitored on silica gel 60 F254 (Merck) plates and visualized with potassium permanganate or ninhydrin and under UV detection ($\lambda = 254 \text{ nm}$, 365 nm). Flash column chromatography was performed using Merck 60/230–400 mesh silica gel. Analytical and semi-preparative reverse-phase HPLC purifications were performed on an Agilent Technologies 1200 series using Jupiter C-18 column ($250 \times 4.60 \text{ mm}$, $5 \mu\text{m}$, 300 \AA ; $250 \times 10.00 \text{ mm}$, $10 \mu\text{m}$, 300 \AA , respectively). Purity grade of final products was determined on a Agilent Technologies 1200 series HPLC using analytical reverse-phase columns (Jupiter C-18, $250 \times 4.60 \text{ mm}$, $5 \mu\text{m}$, 300 \AA).

Reaction yields refer to chromatographically and spectroscopically pure products. Proton-detected (1H , HMBC, HSQC) and carbon-detected NMR spectra were recorded on Bruker instruments of Avance series operating at 300 and 500 MHz and 75 and 125 MHz, respectively. Chemical shifts are expressed in parts per million (ppm) on the delta (δ) scale. The solvent peak was used as internal reference: for 1H -NMR $CDCl_3 = 7.26 \text{ ppm}$ and $CD_3OD = 3.34 \text{ ppm}$; for ^{13}C NMR: $CDCl_3 = 77.0 \text{ ppm}$ and $CD_3OD = 47.7 \text{ ppm}$. Multiplicities are reported as follows: s, singlet; d, doublet; t, triplet; m, multiplet.

Mass spectra (MS) were recorded on a ThermoQuest GC–MS equipped with a Zebtron™ Z5-ms column (capillary in cage column $30 \text{ m} \times 0.25 \text{ mm} \times 0.25 \text{ mm}$) using an electron impact ion source (EI–MS).

The purity of all tested compounds (>95%) were determined by Agilent Technologies 1200 series high-performance liquid chromatography (HPLC) with UV detection at 280 nm (Method: Jupiter C-18 column, $250 \times 4.60 \text{ mm}$, $5 \mu\text{m}$, 300 \AA ; 1.0 mL/min flow rate; 5–100% in 30 min of 0.1% TFA/ CH_3CN -0.1% TFA/ H_2O).

4.2.2. Esterification of boronic acids **26** and **27**

The boronic acids **26** and **27** (0.667 mmol) were dissolved in 6 mL of ethyl acetate and, stirring the solution, pinacol (0.667 mmol) was added. After 4 h the reaction was stopped adding anhydrous Na_2SO_4 (1 g) and $CaCl_2$ (1 g). The mixture was filtered and concentrated *in vacuo* (Yields: 91% of **28** and 89% of **29**).

4.2.3. Synthesis of morpholin-4-yl-[3-(4,4,5,5-tetramethyl-[1,3,2]dioxaborolan-2-yl)-phenyl]-methanone **a**

The pinacol ester **28** (1 equiv.) and morpholine (2 equiv.) were dissolved in DMF. TEA, HOBt and DIC (2 equiv. of each one) were

added. The mixture was leaved at room temperature for 48 h under stirring. When TLC showed the consumption of the pinacol ester **28**, the reaction was stopped adding HCl 1 N (10 mL). The aqueous phase was extracted with ethyl acetate (3 × 10 mL) and the organic phase was washed firstly with a saturate solution of NaHCO₃ and then with brine. The organics were dried over Na₂SO₄, filtered and concentrated in *vacuo*. The crude was purified by flash chromatography (10% diethyl ether/*n*-hexane to 50% diethyl ether/*n*-hexane). Yield: 85%; ¹H-NMR δ (300 MHz; CDCl₃): 7.99 (1H, s), 7.83 (1H, d), 7.45 (1H, d), 7.37 (1H, t), 3.85 (2H, t), 3.70 (4H, m), 3.52 (2H, t), 1.34 (12H, s). ES-MS calcd. for C₁₇H₂₅BNO₄: [M + H]⁺ 318.18; found 318.3.

4.2.4. Synthesis of 4-[2-methoxy-5-(4,4,5,5-tetramethyl-[1,3,2]dioxaborolan-2-yl)-benzyl]-morpholine **1**

Under inert atmosphere (N₂), 1 equiv. of boronic ester **29** was dissolved in anhydrous CH₃OH (1 mL/0.18 mmol of ester). The mixture was kept under stirring at room temperature; anhydrous morpholin (4 equiv.), ZnCl₂ (0.5 equiv.) and NaCNBH₃ (1 equiv.) were added. After 4 h, when the reagents disappeared, the reaction was stopped and 10 mL of an aqueous solution of NaOH 0.1 M was added. After concentration of CH₃OH in *vacuo*, the aqueous phase was extracted with ethyl acetate (3 × 10 mL) and the organics were dried over Na₂SO₄, filtered and concentrated in *vacuo*. The obtained oil was purified on silica gel by flash chromatography (100% *n*-hexane to 50% ethyl acetate/*n*-hexane). Yield: 75%; ¹H-NMR δ (300 MHz; CDCl₃): 7.98 (1H, d), 7.78 (1H, s), 7.24 (1H, d), 4.53 (2H, s), 4.10 (2H, t), 3.93 (3H, s), 3.76 (2H, t), 3.47 (4H, m), 1.35 (12H, s); ES-MS calcd. for C₁₈H₂₉BNO₄: [M + H]⁺ 334.21; found 334.1.

4.2.5. Synthesis of triazoles **22–23** from halides **19–20**: general procedure

The appropriate halide **19–20** (1.1 mmol), 1-bromo-4-ethynylbenzene **18** (1.0 mmol) and sodium azide (1.3 mmol) were suspended in a 1:1 mixture of water and *t*-BuOH (1.5 mL each) in a 10 mL crimp-sealed thick-walled glass tube equipped with a small magnetic stirring bar. Copper wire (0.80 mmol) and copper sulfate solution (1 N, 200 μL) were added to the mixture. Then the mixture was irradiated for 30 min setting the power at 200 W, the temperature at 120 °C, the pressure at 250 psi and the Power Max ON. After completion of the reaction, the vial was cooled to 50 °C by gas jet cooling before it was opened. The mixture was then diluted with water (20 mL) and filtered. The residue was washed with cold water (20 mL), 0.25 N HCl (20 mL) and finally with petroleum ether (20 mL) to furnish the desired triazoles **22–23**.

4.2.6. 4-[4-(4-Bromo-phenyl)-[1,2,3]triazol-1-ylmethyl]-benzoic acid **22**

Yield: 76%; ¹H NMR δ (300 MHz; CD₃OD): 8.07 (2H, d), 7.65 (1H, s), 7.58 (2H, d), 7.45 (2H, d), 7.42 (2H, d), 5.23 (2H, s); HRMS calcd. for C₁₆H₁₃BrN₃O₂: [M + H]⁺ 358.01 and 360.01 (1:1); found and 358.2 and 360.2 (1:1).

4.2.7. 4-[4-(4-Bromo-phenyl)-[1,2,3]triazol-1-ylmethyl]-3-nitro-benzoic acid **23**

Yield: 73%; ¹H NMR δ (300 MHz; CD₃OD): 8.72 (1H, s), 8.35 (1H, s), 8.24 (1H, d), 7.70 (2H, d), 7.56 (2H, d), 7.18 (1H, d), 6.08 (2H, s); HRMS calcd. for C₁₆H₁₂BrN₄O₄: [M + H]⁺ 403.00 and 404.99 (1:1); found 403.3 and 405.3 (1:1).

4.2.8. Synthesis of 4-[4-(4-bromo-phenyl)-[1,2,3]triazole-1-sulfonyl]-benzoic acid **21**

1-Bromo-4-ethynylbenzene **18** (0.60 mmol) and 4-carboxybenzene-sulfonamide **17** (0.50 mmol) were dissolved in 1.00 mL of dry chloroform. 2,6-lutidine (0.60 mmol) and CuI (0.05 mmol) were added and the solution was stirred for 12 h at 0 °C

under inert atmosphere of nitrogen. When TLC analysis indicated complete consumption of the reactants, the reaction mixture was diluted with 10 mL of water. The aqueous layer was extracted with ethyl acetate (3 × 10 mL). The organics were dried over Na₂SO₄, filtered and concentrated in *vacuo*. The crude was purified by flash chromatography (10% diethyl ether/*n*-hexane to 80% diethyl ether/*n*-hexane) and furnished 57% of pure desired triazole **21** as a white powder. ¹H NMR δ (300 MHz; CD₃OD): 8.48 (1H, s), 8.23–8.16 (4H, m), 7.66 (2H, d), 7.53 (2H, d); HRMS calcd. for C₁₅H₁₁BrN₃O₄S: [M + H]⁺ 407.96 and 409.96 (1:1); found 407.8 and 409.8 (1:1).

4.2.9. Suzuki coupling to generate compounds **2–5**; **7–12**; **15–16** and **24–25**: general procedure

In a CEM Discover[®] vial, each of the intermediate **21–23** (1 equiv.), the appropriate boronic acid **a–1** (1.5 equiv.), Pd(dppf)Cl₂ (0.05 equiv.) and CsF (4 equiv.) were placed. Water (500 μL) and THF (500 μL) were added under N₂ atmosphere. The mixture was irradiated for 20–30 min, setting the power at 200 W, the temperature at 120 °C, the pressure at 250 psi and the Power Max ON. At completion of the reaction, the vial was cooled to 50 °C by gas jet cooling before it was opened. After diluting with 10 mL of aqueous solution of HCl 1 N, the aqueous layer was extracted with ethyl acetate (3 × 10 mL). The organics were then dried over Na₂SO₄, filtered and concentrated in *vacuo*. The crude was purified by flash chromatography (10% diethyl ether/*n*-hexane to 40% diethyl ether/*n*-hexane).

4.2.10. 4-[4-(4'-methoxy-3'-morpholin-4-ylmethyl-biphenyl-4-yl)-[1,2,3]triazol-1-ylmethyl]-3-nitro-benzoic acid **2**

Yield: 54%; ¹H NMR δ (300 MHz; CD₃OD): 8.79 (1H, s), 8.56 (1H, s), 8.35 (1H, d, *J* = 7.89 Hz), 8.02 (2H, d, *J* = 8.11 Hz), 7.88 (1H, d, *J* = 8.11 Hz), 7.79 (2H, d, *J* = 7.45 Hz), 7.75 (1H, d, *J* = 7.89 Hz), 7.33 (1H, d, *J* = 8.11 Hz), 6.23 (1H, s), 4.12 (2H, t, *J* = 7.31 Hz), 4.5 (2H, s), 4.01 (3H, s), 3.82 (2H, t, *J* = 6.37 Hz), 3.45 (4H, m); ES-MS calcd. for C₂₈H₂₈N₅O₆: [M + H]⁺ 530.20; found 530.2.

4.2.11. 4-[4-[3'-(Morpholine-4-carbonyl)-biphenyl-4-yl]-[1,2,3]triazol-1-ylmethyl]-3-nitro-benzoic acid **3**

Yield: 56%; ¹H NMR δ (300 MHz; CD₃OD): 8.79 (1H, s), 8.58 (1H, s), 8.35 (1H, d, *J* = 7.89 Hz), 8.02 (2H, d, *J* = 8.11 Hz), 7.88 (1H, d, *J* = 8.11 Hz), 7.79 (2H, d, *J* = 7.89 Hz), 7.75 (1H, s), 7.65 (1H, t, *J* = 6.37 Hz), 7.45 (1H, d, *J* = 8.33 Hz), 7.33 (1H, d, *J* = 8.33 Hz), 6.23 (2H, s), 4.16 (2H, t, *J* = 6.37 Hz), 3.88 (2H, t, *J* = 6.37 Hz), 3.48 (4H, m); ¹³C NMR δ (75 MHz; CD₃OD): 170.1, 165.4, 147.1, 146.2, 140.5, 139.5, 135.6, 134.4, 133.5, 131.6, 130.9, 130.2, 129.9, 128.5, 127.6, 126.8, 126.3, 125.9, 124.3, 121.8, 67.1, 66.2, 50.8, 49.1, 44.4. ES-MS calcd. for C₂₇H₂₄N₅O₆: [M + H]⁺ 514.16; found 514.2.

4.2.12. 4-[4-(4'-amino-biphenyl-4-yl)-[1,2,3]triazol-1-ylmethyl]-3-nitro-benzoic acid **4**

Yield: 49%; ¹H NMR δ (300 MHz; CD₃OD): 8.77 (1H, s), 8.53 (1H, s), 8.26 (1H, d, *J* = 8.11 Hz), 7.88 (2H, d, *J* = 7.67 Hz), 7.70 (2H, d, *J* = 8.33 Hz), 7.49 (2H, d, *J* = 7.33 Hz), 7.24 (1H, d, *J* = 8.11 Hz), 6.81 (2H, d, *J* = 8.11 Hz), 6.22 (2H, s); ¹³C NMR δ (75 MHz; CD₃OD): 165.6, 147.8, 146.8, 139.6, 137.9, 136.9, 134.6, 131.9, 131.5, 130.3, 130.0, 127.5, 126.5, 126.1, 126.1, 122.0, 116.6, 50.9. ES-MS calcd. for C₂₂H₁₈N₅O₄: [M + H]⁺ 416.13; found 416.1.

4.2.13. 4-[4-[4'-(6-dimethylamino-naphthalene-2-sulfonylamino)-biphenyl-4-yl]-[1,2,3]triazol-1-ylmethyl]-3-nitro-benzoic acid **5**

Yield: 51%; ¹H NMR δ (300 MHz; CD₃OD): 8.77 (1H, s), 8.55 (1H, s), 8.24 (2H, d, *J* = 7.67 Hz), 7.89 (1H, d, *J* = 7.67 Hz), 7.71 (2H, d, *J* = 7.89 Hz), 7.55 (2H, d, *J* = 7.67 Hz), 7.50–7.46 (3H, m), 7.32 (2H, d, *J* = 7.67 Hz), 7.13–7.09 (8H, m), 6.95 (1H, d, *J* = 8.11 Hz), 6.85 (1H, d, *J* = 8.11 Hz), 6.19 (2H, s); ¹³C NMR δ (75 MHz; CD₃OD): 167.4, 160.7, 153.5, 149.8, 148.4, 142.6, 141.2, 140.5, 139.1, 138.9, 136.8, 133.8,

132.4, 132.2, 132.0, 131.1, 130.0, 129.2, 129.0, 128.1, 126.0, 125.8, 121.0, 119.0, 117.7, 112.8, 111.1, 52.5, 47.3. ES–MS calcd. for $C_{34}H_{29}N_6O_6S$: $[M + H]^+$ 649.18; found 649.1.

4.2.14. 4'-[1-(4-carboxy-2-nitro-benzyl)-1H-[1,2,3]triazol-4-yl]-biphenyl-3-carboxylic acid 7

Yield: 45%; 1H NMR δ (500 MHz; CD_3OD): 8.77 (1H, s), 8.63 (1H, s), 8.38 (1H, s), 8.37 (1H, d, $J = 8.11$ Hz), 8.08 (1H, d, $J = 7.89$ Hz), 8.04 (1H, d, $J = 7.89$ Hz), 8.09 (2H, d, $J = 8.11$ Hz), 7.89 (2H, d, $J = 8.11$ Hz), 7.70 (1H, t, $J = 7.67$ Hz), 7.35 (1H, d, $J = 8.11$ Hz), 6.22 (2H, s); ^{13}C NMR δ (125 MHz; CD_3OD): 167.3, 165.4, 147.2, 146.4, 139.9, 138.9, 134.0, 133.5, 132.8, 132.3, 130.0, 129.6, 128.8, 128.2, 127.9, 127.4, 126.5, 125.8, 125.4, 121.8, 50.4. ES–MS calcd. for $C_{23}H_{17}N_4O_6$: $[M + H]^+$ 445.11; found 445.1.

4.2.15. 4-[4-(3'-hydroxy-biphenyl-4-yl)-[1,2,3]triazol-1-ylmethyl]-3-nitro-benzoic acid 8

Yield: 42%; 1H NMR δ (300 MHz; CD_3OD): 8.76 (1H, s), 8.23 (1H, d, $J = 7.89$ Hz), 8.12 (1H, s), 7.83 (2H, d, $J = 8.11$ Hz), 7.62 (2H, d, $J = 7.89$ Hz), 7.41 (1H, s), 7.23 (1H, t, $J = 7.67$ Hz), 6.77–6.72 (3H, m), 6.05 (2H, s); ^{13}C NMR δ (75 MHz; CD_3OD): 165.1, 157.5, 147.3, 146.1, 140.3, 139.2, 134.5, 132.1, 130.9, 130.2, 128.4, 128.0, 126.1, 125.9, 125.2, 121.7, 118.3, 116.2, 115.5, 50.8. ES–MS calcd. for $C_{22}H_{17}N_4O_5$: $[M + H]^+$ 417.11; found 417.1.

4.2.16. 4-[4-(3',4',5'-trimethoxy-biphenyl-4-yl)-[1,2,3]triazol-1-ylmethyl]-3-nitro-benzoic acid 9

Yield: 71%; 1H NMR δ (300 MHz; CD_3OD): 8.79 (1H, s), 8.56 (1H, s), 8.34 (1H, d, $J = 7.45$ Hz), 8.00 (2H, d, $J = 8.33$ Hz), 7.81 (2H, d, $J = 8.55$ Hz), 7.31 (1H, d, $J = 8.11$ Hz), 7.01 (2H, s), 6.20 (2H, s), 4.01 (6H, s), 3.80 (3H, s); ^{13}C NMR δ (75 MHz; CD_3OD): 165.4, 153.7, 147.9, 146.1, 141.1, 137.7, 136.6, 134.5, 131.1, 130.3, 129.3, 129.0, 127.6, 126.3, 125.9, 122.2, 104.2, 60.0, 55.5, 50.6. ES–MS calcd. for $C_{25}H_{23}N_4O_7$: $[M + H]^+$ 491.15; found 491.2.

4.2.17. 4-[4-[2'-(2-chloro-5-trifluoromethyl-phenoxy)methyl]-biphenyl-4-yl]-[1,2,3]triazol-1-ylmethyl]-3-nitro-benzoic acid 10

Yield: 62%; 1H NMR δ (300 MHz; CD_3OD): 8.78 (1H, s), 8.48 (1H, s), 8.29 (1H, d, $J = 8.33$ Hz), 7.90 (2H, d, $J = 8.11$ Hz), 7.65 (1H, d, $J = 7.67$ Hz), 7.50 (2H, d, $J = 7.89$ Hz), 7.45–7.37 (6H, m), 7.18 (1H, d, $J = 7.89$ Hz), 6.18 (2H, s), 5.15 (2H, s); ^{13}C NMR δ (75 MHz; CD_3OD): 165.7, 154.4, 148.1, 145.8, 142.2, 140.0, 135.9, 135.1, 133.8, 133.2, 131.5, 131.2, 130.8, 130.5, 130.1, 130.0, 129.9, 129.6, 128.5, 126.2, 125.7, 123.2, 119.0, 118.9, 111.3, 110.1, 69.8, 50.8. ES–MS calcd. for $C_{30}H_{21}ClF_3N_4O_5$: $[M + H]^+$ 609.11; found 609.1.

4.2.18. 3-Nitro-4-[4-(4-thiophen-2-yl-phenyl)-[1,2,3]triazol-1-ylmethyl]-benzoic acid 11

Yield: 54%; 1H NMR δ (300 MHz; CD_3OD): 8.75 (1H, s), 8.55 (1H, s), 8.34 (1H, d, $J = 8.33$ Hz), 7.92 (2H, d, $J = 8.11$ Hz), 7.75 (2H, d, $J = 7.89$ Hz), 7.51 (1H, d, $J = 8.11$ Hz), 7.45 (1H, d, $J = 7.89$ Hz), 7.27 (1H, d, $J = 8.11$ Hz), 7.12 (1H, t, $J = 7.31$ Hz), 6.18 (2H, s); ^{13}C NMR δ (75 MHz; CD_3OD): 165.3, 147.9, 146.1, 141.1, 135.6, 134.3, 133.9, 132.2, 130.4, 130.1, 129.1, 128.8, 126.6, 124.9, 124.2, 121.9, 120.2, 50.7. ES–MS calcd. for $C_{20}H_{15}N_4O_4S$: $[M + H]^+$ 407.07; found 407.0.

4.2.19. 4-[4-(4'-hydroxy-biphenyl-4-yl)-[1,2,3]triazol-1-ylmethyl]-3-nitro-benzoic acid 12

Yield: 47%; 1H NMR δ (300 MHz; CD_3OD): 8.75 (1H, s), 8.53 (1H, s), 8.25 (1H, d, $J = 7.67$ Hz), 7.89 (2H, d, $J = 8.11$ Hz), 7.71 (2H, d, $J = 8.11$ Hz), 7.49 (2H, d, $J = 8.11$ Hz), 7.24 (1H, d, $J = 8.11$ Hz), 6.81 (2H, d, $J = 8.11$ Hz), 6.19 (2H, s); ^{13}C NMR δ (75 MHz; CD_3OD): 165.0, 157.3, 147.9, 166.0, 141.3, 135.0, 134.5, 131.7, 131.1, 130.2, 129.6, 128.2, 126.6, 126.0, 125.9, 121.9, 115.5, 50.7. ES–MS calcd. for $C_{22}H_{17}N_4O_5$: $[M + H]^+$ 417.11; found 417.1.

4.2.20. 4-[4-[2'-(2-chloro-5-trifluoromethyl-phenoxy)methyl]-biphenyl-4-yl]-[1,2,3]triazol-1-ylmethyl]-benzoic acid 15

Yield: 65%; 1H -NMR δ (300 MHz; CD_3OD): 8.41 (1H, s), 8.18 (2H, d, $J = 7.67$ Hz), 7.86 (2H, d, $J = 7.89$ Hz), 7.62 (1H, d, $J = 7.67$ Hz), 7.54–7.42 (8H, m), 7.18 (1H, d, $J = 8.77$ Hz), 7.07 (1H, s), 5.73 (2H, s), 5.11 (2H, s); ^{13}C NMR δ (75 MHz; CD_3OD): 167.1, 154.4, 146.9, 142.2, 141.3, 139.9, 133.7, 131.5, 130.8, 130.4, 130.1, 128.4, 126.0, 125.8, 125.6, 122.6, 119.0, 118.9, 112.3, 111.7, 111.3, 110.0, 108.6, 105.8, 69.8, 53.2. ES–MS calcd. for $C_{30}H_{22}ClF_3N_3O_3$: $[M + H]^+$ 564.12; found 564.2.

4.2.21. 4-[4-[2'-(2-chloro-5-trifluoromethyl-phenoxy)methyl]-biphenyl-4-yl]-[1,2,3]triazole-1-sulfonyl]-benzoic acid 16

Yield: 63%; 1H -NMR δ (300 MHz; CD_3OD): 8.18 (1H, s), 7.86 (2H, d, $J = 8.11$ Hz), 7.63 (1H, d, $J = 7.67$ Hz), 7.55 (2H, d, $J = 8.11$ Hz), 7.45 (1H, t, $J = 5.92$ Hz), 7.43–7.36 (7H, m), 7.18 (1H, d, $J = 8.11$ Hz), 7.09 (1H, s), 5.12 (2H, s); ^{13}C NMR δ (75 MHz; CD_3OD): 167.1, 159.9, 143.6, 142.2, 140.0, 135.9, 135.1, 131.3, 131.1, 133.2, 130.9, 130.6, 130.1, 129.8, 129.7, 128.5, 127.5, 126.8, 125.5, 124.5, 123.1, 118.1, 113.2, 108.3, 69.3. ES–MS calcd. for $C_{29}H_{20}ClF_3N_3O_5S$: $[M + H]^+$ 614.07; found 614.1.

4.2.22. Reduction of nitro-derivative 10 to amine 14: general procedure

A solution of compound **10** and stannous chloride dihydrate (5 equiv.) in ethanol was stirred at 80 °C for about 30 min. The solvent was removed *in vacuo*. Ethyl-acetate (10 mL) was added to the residue and washed with saturated sodium bicarbonate (2 × 10 mL). The organic layer was dried over Na_2SO_4 and concentrated. The obtained compound **14** was directly purified on semi-preparative HPLC (yield: 83%). 1H -NMR δ (300 MHz; CD_3OD): 7.68 (1H, s), 7.18 (2H, d, $J = 8.33$ Hz), 6.97 (1H, d, $J = 7.67$ Hz), 6.89–6.78 (6H, m), 6.72 (2H, d, $J = 7.89$ Hz), 6.54–6.51 (2H, m), 6.42 (1H, s), 4.96 (2H, s), 4.45 (2H, s). ES–MS calcd. for $C_{30}H_{23}ClF_3N_4O_3$: $[M + H]^+$ 579.13; found 579.0.

4.2.23. Oxydation of aldehyde-group to carboxylic acid: general procedure

The advanced intermediates **24** and **25** (1 equiv.) were dissolved in CH_3OH (1 mL) and 0.5 mL of a solution 0.5 M of Na_2HPO_4 in water was added. Finally 0.5 mL of a solution 0.5 M of $KMnO_4$ in water was slowly added dropwise over a period of 1 h. After 1.5 h, the reaction mixture was quenched with 20 mL of HCl 1 M. The aqueous layer was extracted with ethyl acetate (3 × 30 mL) and the organics were dried with Na_2SO_4 , filtered and concentrated *in vacuo*.

4.2.24. 4'-[1-(4-carboxy-2-nitro-benzyl)-1H-[1,2,3]triazol-4-yl]-biphenyl-2-carboxylic acid 6

Yield: 89%; 1H -NMR δ (300 MHz; CD_3OD): 8.08 (1H, s), 7.82 (1H, s), 7.64 (1H, d, $J = 7.89$ Hz), 7.23 (2H, d, $J = 8.11$ Hz), 7.17 (1H, d, $J = 7.45$ Hz), 6.92 (1H, t, $J = 6.79$ Hz), 6.83–6.76 (4H, m), 6.58 (1H, d, $J = 7.45$ Hz), 5.50 (2H, s). ^{13}C NMR δ (75 MHz; CD_3OD): 169.1, 165.5, 147.2, 146.0, 140.6, 139.8, 138.8, 133.2, 132.5, 132.1, 130.3, 130.1, 128.5, 128.1, 126.9, 125.8, 125.4, 121.9, 50.8. ES–MS calcd. for $C_{23}H_{17}N_4O_6$: $[M + H]^+$ 445.11; found 445.1.

4.2.25. 4'-[1-(4-carboxy-2-nitro-benzyl)-1H-[1,2,3]triazol-4-yl]-biphenyl-4-carboxylic acid 13

Yield: 86%; 1H -NMR δ (300 MHz; CD_3OD): 8.08 (1H, s), 7.86 (1H, s), 7.64 (1H, d, $J = 7.67$ Hz), 7.48 (2H, d, $J = 8.11$ Hz), 7.33 (2H, d, $J = 8.33$ Hz), 7.17 (1H, d, $J = 8.11$ Hz), 6.95 (2H, d, $J = 8.11$ Hz), 6.59 (2H, d, $J = 8.11$ Hz), 5.50 (2H, s). ^{13}C NMR δ (75 MHz; CD_3OD): 167.1, 165.5, 147.2, 146.1, 140.5, 139.9, 138.9, 134.1, 133.8, 132.6, 130.2, 130.0, 128.2, 128.0, 126.9, 125.9, 121.9, 50.7. ES–MS calcd. for $C_{23}H_{17}N_4O_6$: $[M + H]^+$ 445.11; found 445.0.

4.3. Bioactivity assays

4.3.1. Assay systems and materials

Dulbecco's Modified Eagle Medium (DMEM)/high glucose (4.5 g/L) medium, penicillin, streptomycin, trypsin/ethylenediaminetetraacetate (EDTA) solution, and LSM 1077 lymphocyte separation medium were obtained from PAA (Pasching, Austria). IL-1 β was obtained from ReproTech (Hamburg, Germany). Fetal calf serum (FCS), phenylmethylsulfonyl fluoride (PMSF), leupeptin, soybean trypsin inhibitor (STI), glutathione (reduced), PGB₁, lysozyme, Ca²⁺-ionophore A23187, and arachidonic acid were obtained from Sigma–Aldrich (Deisenhofen, Germany). MK886 and 11 β -PGE₂ were obtained from Cayman Chemical (Ann Arbor, MI). PGH₂, adenosine triphosphate (ATP), isopropyl- β -D-1-thiogalactopyranoside (IPTG), and dextrane were obtained from Larodan (Malmö, Sweden), Roche Diagnostics (Mannheim, Germany), AppliChem (Darmstadt, Germany), and Fluka (Neu-Ulm, Germany), respectively. A549 cells were provided by the Karolinska Institute (Stockholm, Sweden). Leukocyte concentrates from human healthy volunteers were provided by Institute of Transfusion Medicine, University Hospital Jena, Germany.

4.3.2. Cell culture

A549 cells were grown in DMEM/high glucose (4.5 g/mL) medium supplemented with heat-inactivated FCS (10%, v/v), penicillin (100 U/mL) and streptomycin (100 μ g/mL). After three days, confluent cells were detached using 1x trypsin/EDTA and reseeded with a density of 1 \times 10⁵ cells/ml medium.

4.3.3. Preparation of crude mPGES-1 in microsomes of A549 cells and determination of mPGE₂ synthase activity

Preparation of A549 cells and determination of mPGES-1 activity was performed as described previously [34]. In brief, A549 cells were treated with 1 ng/mL interleukin-1 β for 48 h at 37 °C and 5% CO₂. After sonification, the homogenate was subjected to differential centrifugation at 10,000 \times g for 10 min and 174,000 \times g for 1 h at 4 °C. The pellet (microsomal fraction) was resuspended in 1 mL homogenization buffer (0.1 M potassium phosphate buffer pH 7.4, 1 mM phenylmethanesulphonyl fluoride, 60 μ g/mL soybean trypsin inhibitor, 1 μ g/mL leupeptin, 2.5 mM glutathione, and 250 mM sucrose), and the total protein concentration was determined. Microsomal membranes were diluted in potassium phosphate buffer (0.1 M, pH 7.4) containing 2.5 mM glutathione. Test compounds or vehicle were added, and after 15 min at 4 °C, the reaction (100 μ l total volume) was initiated by addition of PGH₂ (20 μ M, final concentration, unless stated otherwise). After 1 min at 4 °C, the reaction was terminated using stop solution (100 μ l; 40 mM FeCl₂, 80 mM citric acid, and 10 μ M of 11 β -PGE₂ as internal standard). PGE₂ was separated by solid phase extraction and analyzed by RP-HPLC as described [34].

4.3.4. Expression and purification of human 5-LO from *Escherichia coli* (*E. coli*)

E. coli MV1190 was transformed with pT3-5-LO plasmid, and recombinant 5-LO protein was expressed at 27 °C as described [47]. Cells were lysed in 50 mM triethanolamine/HCl pH 8.0, 5 mM EDTA, soybean trypsin inhibitor (60 μ g/mL), 1 mM phenylmethanesulphonyl fluoride, and lysozyme (500 μ g/mL), homogenized by sonication (3 \times 15 s), and centrifuged at 40,000 \times g for 20 min at 4 °C. The 40,000 \times g supernatant (S40) was applied to an ATP-agarose column to partially purify 5-LO as described previously [47]. Semi-purified 5-LO was immediately used for activity assays.

4.3.5. Determination of 5-LO activity in cell-free assay

Aliquots of semi-purified 5-LO were diluted with ice-cold PBS containing 1 mM EDTA, and 1 mM ATP was added. Samples were

pre-incubated with the test compounds as indicated. After 10 min at 4 °C, samples were pre-warmed for 30 s at 37 °C, and 2 mM CaCl₂ plus 20 μ M AA was added to start 5-LO product formation. The reaction was stopped after 10 min at 37 °C by addition of 1 mL ice-cold methanol, and the formed metabolites were analyzed by RP-HPLC as described [48]. 5-LO products include the all-trans isomers of LTB₄ and 5(S)-hydro(pero)xy-6-*trans*-8,11,14-*cis*-eicosatetraenoic acid.

4.3.6. Isolation of neutrophils and determination of 5-LO activity in neutrophils

Neutrophils were freshly isolated from leukocyte concentrates obtained at the Institute of Transfusion Medicine, University Hospital Jena, Germany, as described [49]. In brief, venous blood was taken from healthy adult donors that did not take any medication for at least 7 days, and leukocyte concentrates were prepared by centrifugation (4000 \times g, 20 min, 20 °C). Neutrophils were immediately isolated from the pellet after centrifugation on Nycoprep cushions, and hypotonic lysis of erythrocytes was performed. Neutrophils were finally resuspended in PBS pH 7.4 (PBS) containing 1 mg/mL glucose and 1 mM CaCl₂ (PGC buffer) (purity > 96–97%).

Freshly isolated neutrophils (1 \times 10⁷/mL PGC buffer) were pre-incubated with the test compounds for 15 min at 37 °C and 5-LO product formation was started by addition of 2.5 μ M ionophore A23187 plus 20 μ M AA. After 10 min at 37 °C, the reaction was stopped with 1 mL of methanol and 30 μ l of 1 N HCl, and then, 200 ng PGB₁ and 500 μ l PBS were added. Formed 5-LO metabolites were extracted and analyzed by HPLC as described [8]. 5-LO products include LTB₄ and its all-trans isomers, and 5(S)-hydro(pero)xy-6-*trans*-8,11,14-*cis*-eicosatetraenoic acid. Cysteinyl-LTs C₄, D₄, and E₄ were not detected, and oxidation products of LTB₄ were not determined.

4.3.7. Statistics

Data are expressed as mean \pm SE. IC₅₀ values were graphically calculated from measurements at 4–5 different concentrations of the compounds using SigmaPlot 9.0 (Systat Software Inc., San Jose, USA). The program Graphpad Instat (Graphpad Software Inc., San Diego, CA) was used for statistical comparisons. Statistical evaluation of the data was performed by one-way ANOVAs for independent or correlated samples followed by Tukey HSD post-hoc tests. Where appropriate, Student's *t* test for paired and correlated samples was applied. A *P* value of <0.05 was considered significant.

Acknowledgments

Financial support by the University of Salerno and by Ministero dell'Istruzione, dell'Università e della Ricerca (MIUR), PRIN 2009 "Design, conformational and configurational analysis of novel molecular platforms". Both the institutions are gratefully acknowledged.

References

- [1] P. McGettigan, D. Henry, Cardiovascular risk and inhibition of cyclooxygenase: a systematic review of the observational studies of selective and nonselective inhibitors of cyclooxygenase 2, *JAMA* 296 (2006) 1633–1644.
- [2] F. Buttgerit, G.R. Burmester, L.S. Simon, Gastrointestinal toxic side effects of nonsteroidal anti-inflammatory drugs and cyclooxygenase-2-specific inhibitors, *Am. J. Med.* 110 (Suppl. 3A) (2001) 13S–19S.
- [3] H.F. Cheng, R.C. Harris, Renal effects of non-steroidal anti-inflammatory drugs and selective cyclooxygenase-2 inhibitors, *Curr. Pharm. Des.* 11 (2005) 1795–1804.
- [4] P.J. Jakobsson, S. Thoren, R. Morgenstern, B. Samuelsson, Identification of human prostaglandin E synthase: a microsomal, glutathione-dependent, inducible enzyme, constituting a potential novel drug target, *Proc. Natl. Acad. Sci. U.S.A.* 96 (1999) 7220–7225.

- [5] R.W. Friesen, J.A. Mancini, Microsomal prostaglandin E2 synthase-1 (mPGES-1): a novel anti-inflammatory therapeutic target, *J. Med. Chem.* 51 (2008) 4059–4067.
- [6] M. Murakami, H. Naraba, T. Tanioka, N. Semmyo, Y. Nakatani, F. Kojima, T. Ikeda, M. Fueki, A. Ueno, S. Oh, I. Kudo, Regulation of prostaglandin E2 biosynthesis by inducible membrane-associated prostaglandin E2 synthase that acts in concert with Cyclooxygenase-2, *J. Biol. Chem.* 275 (2000) 32783–32792.
- [7] A. Koeberle, O. Werz, Inhibitors of the microsomal prostaglandin E(2) synthase-1 as alternative to non steroidal anti-inflammatory drugs (NSAIDs)—a critical review, *Curr. Med. Chem.* 16 (2009) 4274–4296.
- [8] R. De Simone, M.G. Chini, I. Bruno, R. Riccio, D. Mueller, O. Werz, G. Bifulco, Structure-based discovery of inhibitors of microsomal prostaglandin E(2) Synthase-1, 5-Lipoxygenase and 5-Lipoxygenase-activating protein: promising hits for the development of new anti-inflammatory agents, *J. Med. Chem.* 54 (2011) 1565–1575.
- [9] M.C. Monti, M.G. Chini, L. Margarucci, R. Riccio, G. Bifulco, A. Casapullo, The binding mode of Cladocoran A to the human group IIA phospholipase A(2), *Chembiochem* 12 (2011) 2686–2691.
- [10] M.C. Monti, M.G. Chini, L. Margarucci, A. Tosco, R. Riccio, G. Bifulco, A. Casapullo, The molecular mechanism of human group IIA phospholipase A2 inactivation by bolinaquinone, *J. Mol. Recognit.* 22 (2009) 530–537.
- [11] V. Sepe, G. Bifulco, B. Renga, C. D'Amore, S. Fiorucci, A. Zampella, Discovery of sulfated sterols from marine invertebrates as a new class of marine natural antagonists of farnesoid-X-receptor, *J. Med. Chem.* 54 (2011) 1314–1320.
- [12] S. De Martino, R. Ummarino, M.V. D'auria, M.G. Chini, G. Bifulco, B. Renga, C. D'Amore, S. Fiorucci, C. Debitus, A. Zampella, Theonellasterols and conicasterols from *Theonella swinhoei*. Novel marine natural ligands for human nuclear receptors, *J. Med. Chem.* 54 (2011) 3065–3075.
- [13] C. Festa, S. De Martino, M.V. D'auria, G. Bifulco, B. Renga, S. Fiorucci, S. Petek, A. Zampella, Solomonsterols A and B from *Theonella swinhoei*. The first example of C-24 and C-23 sulfated sterols from a marine source endowed with a PXR agonistic activity, *J. Med. Chem.* 54 (2011) 401–405.
- [14] S. Cipriani, A. Mencarelli, M.G. Chini, E. Distrutti, B. Renga, G. Bifulco, F. Baldelli, A. Donidi, S. Fiorucci, The bile acid receptor GPBAR-1 (TGR5) modulates integrity of intestinal barrier and immune response to experimental colitis, *PLoS One* 6 (25637) (2011) 1–11.
- [15] S. Terracciano, M.G. Chini, R. Riccio, I. Bruno, G. Bifulco, *ChemMedChem* 7 (2012) 694–702.
- [16] C. Jegerschold, S.C. Pawelzik, P. Purhonen, P. Bhakat, K.R. Gheorghe, N. Gyobu, K. Mitsuoka, R. Morgenstern, P.J. Jakobsson, H. Hebert, Structural basis for induced formation of the inflammatory mediator prostaglandin E2, *Proc. Natl. Acad. Sci. U.S.A.* 105 (2008) 11110–11115.
- [17] G.M. Morris, R. Huey, W. Lindstrom, M.F. Sanner, R.K. Belew, D.S. Goodsell, A.J. Olson, AutoDock4 and AutoDockTools4: automated docking with selective receptor flexibility, *J. Comput. Chem.* 30 (2009) 2785–2791.
- [18] P.J. Holm, P. Bhakat, C. Jegerschold, N. Gyobu, K. Mitsuoka, Y. Fujiyoshi, R. Morgenstern, H. Hebert, Structural basis for detoxification and oxidative stress protection in membranes, *J. Mol. Biol.* 360 (2006) 934–945.
- [19] S. Thoren, R. Weinander, S. Saha, C. Jegerschold, P.L. Pettersson, B. Samuelsson, H. Hebert, M. Hamberg, R. Morgenstern, P.J. Jakobsson, Human microsomal prostaglandin E synthase-1: purification, functional characterization, and projection structure determination, *J. Biol. Chem.* 278 (2003) 22199–22209.
- [20] A. Hamza, M.D. AbdulHameed, C.G. Zhan, Understanding microscopic binding of human microsomal prostaglandin E synthase-1 with substrates and inhibitors by molecular modeling and dynamics simulation, *J. Phys. Chem. B* 112 (2008) 7320–7329.
- [21] L. Xing, R.G. Kurumbail, R.B. Frazier, M.S. Davies, H. Fujiwara, R.A. Weinberg, J.K. Gierse, N. Caspers, J.S. Carter, J.J. McDonald, W.M. Moore, M.L. Vazquez, Homo-timeric structural model of human microsomal prostaglandin E synthase-1 and characterization of its substrate/inhibitor binding interactions, *J. Comput.-Aided Mol. Des.* 23 (2009) 13–24.
- [22] S. He, L. Lai, Molecular docking and competitive binding study discovered different binding modes of microsomal prostaglandin E Synthase-1 inhibitors, *J. Chem. Inf. Model.* 51 (2011) 3254–3261.
- [23] E.B. Prage, S.C. Pawelzik, L.S. Busenlehner, K. Kim, R. Morgenstern, P.J. Jakobsson, R.N. Armstrong, Location of inhibitor binding sites in the human inducible prostaglandin E synthase, *MPGES1*, *Biochemistry* 50 (2011) 7684–7693.
- [24] A. Hamza, M. Tong, M.D. AbdulHameed, J. Liu, A.C. Goren, H.H. Tai, C.G. Zhan, Understanding microscopic binding of human microsomal prostaglandin E synthase-1 (mPGES-1) trimer with substrate PGH₂ and cofactor GSH: insights from computational alanine scanning and site-directed mutagenesis, *J. Phys. Chem.* 114 (2010) 5605–5616.
- [25] S.C. Pawelzik, N.R. Uda, L. Spahiu, C. Jegerschold, P. Stenberg, H. Hebert, R. Morgenstern, P.J. Jakobsson, Identification of key residues determining species differences in inhibitor binding of microsomal prostaglandin E synthase-1, *J. Biol. Chem.* 285 (2010) 29254–29261.
- [26] J.P. Iyer, P.K. Srivastava, R. Dev, S.G. Dastidar, A. Ray, Prostaglandin E(2) synthase inhibition as a therapeutic target, *Expert Opin. Ther. Targets* 13 (2009) 849–865.
- [27] R. Huisgen, 1,3-Dipolar cycloaddition – introduction, survey, mechanism, in: A. Padwa (Ed.), *1,3-Dipolar Cycloaddition Chemistry*, Wiley, New York, 1984, pp. 1–176.
- [28] N. Miyaoura, K. Yamada, A. Suzuki, A new stereospecific cross-coupling by the palladium-catalyzed reaction of 1-alkenylboranes with 1-alkenyl or 1-alkynyl halides, *Tetrahedron Lett.* 20 (1979) 3437–3440.
- [29] M. Whiting, V.V. Fokin, Copper-catalyzed reaction cascade: direct conversion of alkynes into N-sulfonylazetid-2-imines, *Angew. Chem. Int. Ed. Engl.* 45 (2006) 3157–3161.
- [30] E.J. Yoo, M. Ahlquist, S.H. Kim, I. Bae, V.V. Fokin, K.B. Sharpless, S. Chang, Copper-catalyzed synthesis of N-sulfonyl-1,2,3-triazoles: controlling selectivity, *Angew. Chem. Int. Ed. Engl.* 46 (2007) 1730–1733.
- [31] P. Appukkuttan, W. Dehaen, V.V. Fokin, E.E. Van der, A microwave-assisted click chemistry synthesis of 1,4-disubstituted 1,2,3-triazoles via a copper(I)-catalyzed three-component reaction, *Org. Lett.* 6 (2004) 4223–4225.
- [32] V.V. Rostovtsev, L.G. Green, V.V. Fokin, K.B. Sharpless, A stepwise Huisgen cycloaddition process: copper(I)-catalyzed regioselective "ligation" of azides and terminal alkynes, *Angew. Chem. Int. Ed. Engl.* 41 (2002) 2596–2599.
- [33] M. Aquino, M.D. Guerrero, I. Bruno, M.C. Terencio, M. Paya, R. Riccio, Development of a second generation of inhibitors of microsomal prostaglandin E synthase 1 expression bearing the gamma-hydroxybutenolide scaffold, *Bioorg. Med. Chem.* 16 (2008) 9056–9064.
- [34] A. Koeberle, H. Zettl, C. Greiner, M. Wurglics, M. Schubert-Zsilavecz, O. Werz, Pirinixic acid derivatives as novel dual inhibitors of microsomal prostaglandin E2 synthase-1 and 5-lipoxygenase, *J. Med. Chem.* 51 (2008) 8068–8076.
- [35] D. Claveau, M. Sirinyan, J. Guay, R. Gordon, C.C. Chan, Y. Bureau, D. Riendeau, J.A. Mancini, Microsomal prostaglandin E synthase-1 is a major terminal synthase that is selectively up-regulated during cyclooxygenase-2-dependent prostaglandin E2 production in the rat adjuvant-induced arthritis model, *J. Immunol.* 170 (2003) 4738–4744.
- [36] O. Rådmark, B. Samuelsson, Microsomal prostaglandin E synthase-1 and 5-lipoxygenase: potential drug targets in cancer, *J. Intern. Med.* 268 (2010) 5–14.
- [37] M. Hieke, C. Greiner, M. Dittrich, F. Reisen, G. Schneider, M. Schubert-Zsilavecz, O. Werz, Discovery and biological evaluation of a novel class of dual microsomal prostaglandin E2 synthase-1/5-lipoxygenase inhibitors based on 2-[(4,6-diphenethoxypyrimidin-2-yl)thio]hexanoic acid, *J. Med. Chem.* 54 (2011) 4490–4507.
- [38] N.C. Gilbert, S.G. Bartlett, M.T. Waight, D.B. Neau, W.E. Boeglin, A.R. Brash, M.E. Newcomer, The structure of human 5-lipoxygenase, *Science* 331 (2011) 217–219.
- [39] O. Werz, 5-lipoxygenase: cellular biology and molecular pharmacology, *Curr. Drug Targets Inflamm. Allergy* 1 (2002) 23–44.
- [40] C. Pergola, O. Werz, 5-Lipoxygenase inhibitors: a review of recent developments and patents, *Expert Opin. Ther. Patents* 20 (2010) 355–375.
- [41] C. Charlier, J.P. Henichart, F. Durant, J. Wouters, Structural insights into human 5-lipoxygenase inhibition: combined ligand-based and target-based approach, *J. Med. Chem.* 49 (2006) 186–195.
- [42] L. Fang-Yu, J.T. Yufeng, Structure-based fragment hopping for lead optimization using predocked fragment database, *J. Chem. Inf. Model.* 51 (2011) 1703–1715.
- [43] Y. Li, S.H. Chen, T.M. Ou, J.H. Tan, D. Li, L.Q. Gu, Z.S. Huang, Synthesis and characterization of nimesulide derivatives for dual enzyme inhibitors of both cyclooxygenase-1/2 and 5-lipoxygenase, *Bioorg. Med. Chem.* 19 (2011) 2074–2083.
- [44] G. Eren, A. Macchiarulo, E. Banoglu, From molecular docking to 3D-Quantitative structure-activity relationships (3D-QSAR): insights into the binding mode of 5-Lipoxygenase inhibitors, *Mol. Inf.* 31 (2012) 123–134.
- [45] O. Trott, A.J. Olson, AutoDock Vina: Improving the speed and accuracy of docking with a new scoring function, efficient optimization, and multi-threading, *J. Comput. Chem.* 31 (2010) 455–461.
- [46] M.F. Sanner, Python: a programming language for software integration and development, *J. Mol. Graphics Modell.* 17 (1999) 57–61.
- [47] L. Fischer, D. Szellas, O. Rådmark, D. Steinhilber, O. Werz, Phosphorylation- and stimulus-dependent inhibition of cellular 5-lipoxygenase activity by nonredox-type inhibitors, *FASEB J.* 17 (2003) 949–951.
- [48] O. Werz, E. Burkert, B. Samuelsson, O. Rådmark, D. Steinhilber, Activation of 5-lipoxygenase by cell stress is calcium independent in human polymorphonuclear leukocytes, *Blood* 99 (2002) 1044–1052.
- [49] C. Pergola, G. Dodt, A. Rossi, E. Neunhoffer, B. Lawrenz, H. Northoff, B. Samuelsson, O. Rådmark, L. Sautebin, O. Werz, ERK-mediated regulation of leukotriene biosynthesis by androgens: a molecular basis for gender differences in inflammation and asthma, *Proc. Natl. Acad. Sci. U. S. A.* 105 (2008) 19881–19886.